

# Motion Focus Recognition in Fast-Moving Egocentric Video

Daniel Hong<sup>1</sup>, James Tribble<sup>1</sup>, Hao Wang<sup>1\*</sup>, Chaoyi Zhou<sup>1</sup>, Ashish Bastola<sup>1</sup>,  
Siyu Huang<sup>1</sup>, and Abolfazl Razi<sup>1</sup>

<sup>1</sup>Clemson University, SC, USA

{sienh, jjtribb, hao9, chaoyiz, abastol, siyuh, arazi}@clemson.edu

## Abstract

From Vision-Language-Action (VLA) systems to robotics, existing egocentric datasets primarily focus on action recognition tasks, while largely overlooking the inherent role of motion analysis in sports and other fast-movement scenarios. To bridge this gap, we propose a real-time motion focus recognition method that estimates the subject's locomotion intention from any egocentric video. Our approach leverages the foundation model for camera pose estimation and introduces system-level optimizations to enable efficient and scalable inference. Evaluated on a collected egocentric action dataset, our method achieves real-time performance with manageable memory consumption through a sliding batch inference strategy. This work makes motion-centric analysis practical for edge deployment and offers a complementary perspective to existing egocentric studies on sports and fast-movement activities. Our code and dataset are available on: <https://arazi2.github.io/aisends.github.io/project/VisionGPT>

## 1. Introduction

In fast human movement, egocentric perception is fundamentally more challenging than vision tasks developed for autonomous vehicles or rigid robotic platforms [6]. Unlike vehicle-mounted cameras operating under stable kinematic constraints, egocentric video is shaped by frequent head movements, body sway, and intentional gaze shifts, leading to unstable viewpoints and noisy motion feedback [2]. In such settings, common assumptions, such as image-center relevance and consistent camera orientation, break down, making reliable real-time ego-motion estimation particularly challenging [4].

Most existing attention and relevance estimation methods for egocentric vision rely primarily on static or appearance-based saliency to identify important regions and objects [5]. While effective in relatively stable settings, such approaches can introduce substantial bias in

high-motion environments, as visually salient but motion-inconsistent objects often appear only transiently and disappear within a few frames. Consequently, static saliency fails to capture the temporally persistent information that is most informative for understanding ego-motion and short-term movement intent [9].



Figure 1. (a) Selected frame from the dataset collected during the winter season. (i) is the raw city street image, (ii) is the motion-focus map, and (iii) is the motion-guided depth map. (b) is the example camera system for data capturing.

To address this limitation, we propose a real-time motion focus recognition method that estimates human locomotion trends from egocentric video while being robust to irregular camera movement noise induced by natural head and body movements. Our approach is grounded in physical priors of camera pose dynamics and does not require additional training, enabling flexible motion trend estimation under highly dynamic viewpoints [7]. Furthermore, the proposed method can be embedded into arbitrary camera pose estimation frameworks with minimal computational cost, supporting real-time deployment on resource-constrained systems in fast-movement settings.

Specifically, we adopt the camera pose prediction from an existing foundation model and apply deep systematic optimization for real-time egocentric motion recognition [3]. To overcome the shortage of existing egocentric datasets in fast-movement scenarios, we collect a lightweight egocentric action dataset and incorporate real camera intrinsics as physical constraints for error compensation, enabling more stable motion focus recognition under real-world cap-

\*Corresponding author

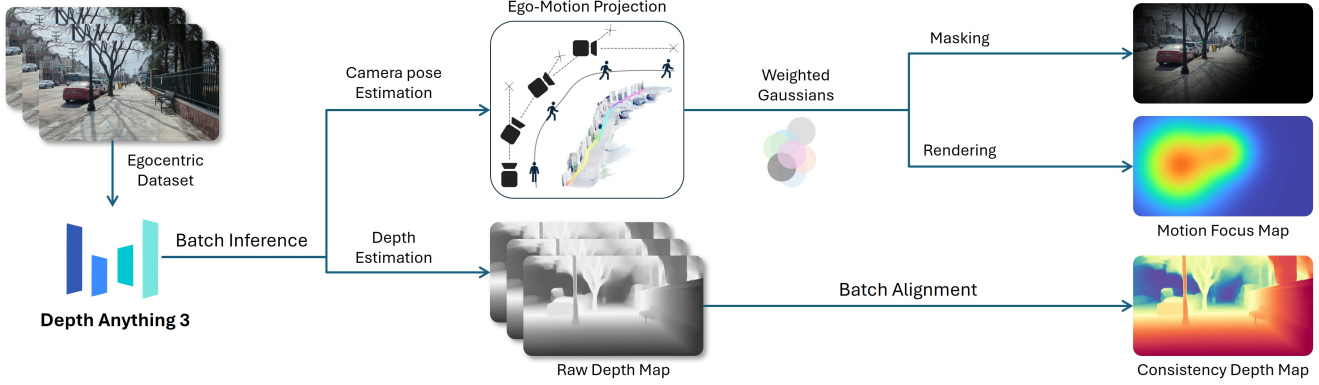


Figure 2. Framework for motion focus prediction and projection.

ture conditions. Experimental results show that the predicted motion focus highlights the videographer’s locomotion trend.

## 2. Method

### 3. Data Collection

We collect an egocentric action video dataset through in-person acquisition to capture realistic human locomotion under dynamic environments. All videos are recorded using a single monocular handheld mobile phone carried by a walking subject, resulting in camera motion that reflects natural translation, head turns, and body-induced perturbations.

Scene	Clips	Resolution	FPS	Total length	Total Frames
Suburban	42	960x544	30	37 mins	65934
City	56	1920x1080	30	79 mins	5464
Town	36	3840x2160	30	24 mins	21528
Campus	72	1920x1080	60	75 mins	269550

Table 1. Collected egocentric video clips for motion analysis tasks.

Data is collected during winter conditions across diverse and challenging environments, including outdoor sidewalks and pedestrian walkways with uneven surfaces and icy roads, as shown in Figure 1. The dataset further includes multiple locomotion patterns, such as walking, scooter riding, and biking, together with motion variations including turning, slowing down, and brief stopping, producing rich ego-motion dynamics. In total, the dataset contains action video clips captured at varying resolutions and frame rates, as summarized in Table 1.

### 3.1. System Optimization for Real-Time Inference

Since Depth Anything 3 is primarily designed for offline inference in industrial applications [3], processing an entire long video in one pass quickly exceeds GPU memory.

During our testing on a 24 GB desktop GPU, sequences exceeding 1000 frames fail due to running out of memory. To avoid this, we split the video into overlapping batches, perform inference per batch, and align them temporally. This reduces peak memory usage while preserving a complete, consistent sequence of depth maps and camera poses, as shown in Figure 3.

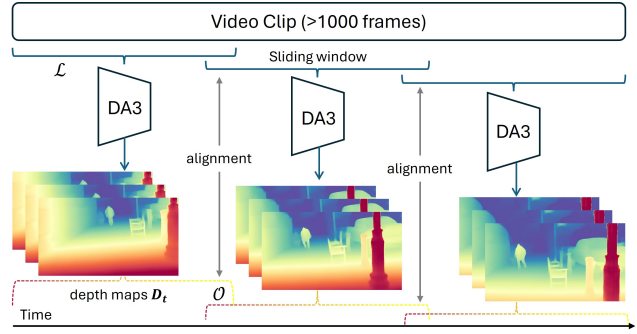


Figure 3. Depth alignment in the real-time inference. We applied a sliding window for consecutive inference in real time.

Specifically, to handle extended video streams  $\{\mathbf{I}_t\}$  under memory constraints while maintaining real-time performance, we adopt a sliding-window inference strategy. The continuous stream is partitioned into overlapping segments (batches) of size  $\mathcal{L}$ , where consecutive windows share  $\mathcal{O}$  frames to ensure temporal context, as shown in Figure 3.

For each batch, the model predicts depth maps  $\{D_t\}$  and camera extrinsics  $\{\mathbf{T}_t^{w \rightarrow c}\}$  in a local coordinate frame. To resolve the coordinate ambiguity between consecutive batches, we perform an incremental anchoring process. Let  $t_{anchor}$  denote the transition frame shared by the current and previous windows. We compute a rigid transformation to align the current batch’s local origin to the terminal pose of the previous trajectory, effectively stitching the segments into a unified world coordinate system.

Specifically, to maintain the physical consistency of the motion, we lock the gravity-aligned rotation (pitch and

roll) and propagate only the horizontal yaw and translation across batch boundaries. This incremental anchoring avoids the global drift typical of large-scale Sim(3) optimization while preserving the predictive power of the foundation model for long-range navigation [3]. Following the alignment, only the newly processed, non-overlapping frames are emitted, ensuring a continuous and temporally coherent flow of depth and pose estimates for downstream motion analysis.

Model	Resolution	Batch Size	FPS	GPU Mem.
DA3 Base	504	60	31.53	8113 MB
DA3 Base	384	60	34.01	5556 MB
DA3 Base	384	30	28.65	4501 MB
DA3 Small	504	60	32.95	4609 MB
DA3 Small	384	60	38.44	3437 MB
DA3 Small	504	30	35.87	3677 MB
DA3 Small	384	30	32.32	3064 MB

Table 2. Performance of DA3.

We evaluate the batch inference strategy under different configurations to assess its suitability for real-time deployment. As shown in Table 2, the DA3 base model achieves 31.53 FPS with approximately 8 GB GPU memory at a batch size of 60, and further improves to 34.01 FPS with reduced memory usage when the resolution is lowered to 384 px. While smaller batch sizes reduce memory consumption, they also lead to decreased throughput due to increased I/O and scheduling overhead. By replacing the base model with the DA3 small variant, our framework maintains stable real-time performance above 30 FPS with GPU memory usage below 5 GB, enabling practical deployment on consumer-grade hardware.

### 3.2. Motion Focus Recognition

To enable motion-aware prioritization in fast movements, we introduce a lightweight Motion Focus Recognition module that estimates the impact region induced by the user’s locomotion. The core intuition is that the acceleration vector induced by camera translation, when projected onto the image plane, provides a physically grounded focus of attention indicating where near-field interactions or potential collisions are most likely to occur [1, 7, 8].

Let  $\mathbf{T}_t^{w \rightarrow c} \in \mathbb{R}^{4 \times 4}$  denote the camera pose at time  $t$ , expressed as a world-to-camera transformation. We first recover the camera positions in the world coordinate system by inverting the poses:

$$\mathbf{T}_t^{c \rightarrow w} = (\mathbf{T}_t^{w \rightarrow c})^{-1}, \quad \mathbf{p}_t = \mathbf{T}_t^{c \rightarrow w}[1:3, 4]. \quad (1)$$

To characterize the dynamic trend of the trajectory, we compute the discrete acceleration vector in world space,  $\mathbf{a}_w$ , by considering three consecutive pose samples:

$$\mathbf{v}_t = \mathbf{p}_t - \mathbf{p}_{t-1}, \quad \mathbf{v}_{t-1} = \mathbf{p}_{t-1} - \mathbf{p}_{t-2} \quad (2)$$

$$\mathbf{a}_w = \mathbf{v}_t - \mathbf{v}_{t-1} = \mathbf{p}_t - 2\mathbf{p}_{t-1} + \mathbf{p}_{t-2}. \quad (3)$$

To align this motion trend with the user’s current egocentric perspective, the acceleration vector is transformed from the world frame into the local camera coordinate frame:

$$\mathbf{a}_c = \mathbf{R}_t^{w \rightarrow c} \mathbf{a}_w, \quad (4)$$

where  $\mathbf{R}_t^{w \rightarrow c}$  is the rotation matrix of  $\mathbf{T}_t^{w \rightarrow c}$ . The local vector  $\mathbf{a}_c = (a_x, a_y, a_z)^\top$  encapsulates the directional change of motion relative to the optical axis.

Assuming a pinhole camera model with an intrinsic matrix

$$\mathbf{K} = \begin{bmatrix} f_x & 0 & c_x \\ 0 & f_y & c_y \\ 0 & 0 & 1 \end{bmatrix}, \quad (5)$$

We project the motion direction onto the image plane to obtain an estimated impact point:

$$u_{acc} = c_x + f_x \frac{a_x}{a_z}, \quad v_{acc} = c_y + f_y \frac{a_y}{a_z}. \quad (6)$$

The coordinate  $(u_{acc}, v_{acc})$  serves as the center of a motion-induced saliency map. Unlike velocity-based projection, this acceleration-based focus effectively anticipates the user’s intent to turn or decelerate, as shown in Figure 4.



Figure 4. Motion focus calculation process. We first calculate the camera center and project the acceleration vector to the  $k$ th frame. Then we aggregate  $K$  camera centers and apply Gaussian kernels for rendering. The final results represent the camera movement trends, which aligned with the defined motion focus.

As shown in Figure 4, we then construct a motion focus map by aggregating  $K$  (e.g., 15) motion points in the image plane. Each motion point contributes a Gaussian kernel centered at its projected pixel location, with the kernel spread modulated by the corresponding motion magnitude to reflect its spatial influence. The final focus map is obtained by summing all kernels and normalizing the result:

$$M(u, v) = \frac{1}{Z} \sum_{i=1}^K \exp \left( -\frac{(u - u_i)^2 + (v - v_i)^2}{2(\sigma s_i)^2} \right), \quad (7)$$

where  $(u_i, v_i)$  denotes the  $i$ -th motion point,  $s_i$  its motion magnitude,  $\sigma$  a scale factor, and  $Z$  a normalization constant.

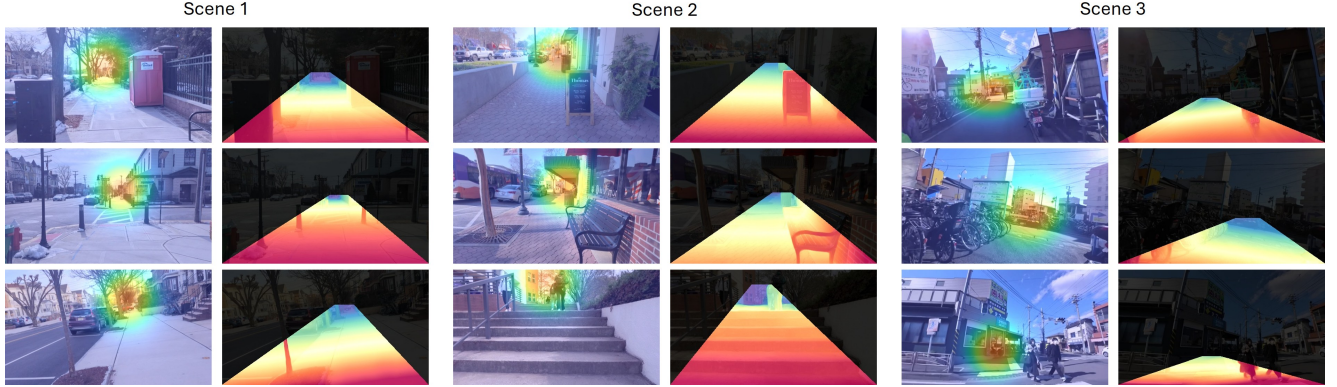


Figure 5. Visualization of motion focus. Left: raw image with predicted motion focus map; Right: depth map guided by motion direction.

The resulting motion focus is characterized by both its spatial location in the image and its associated depth and forward velocity, allowing the system to prioritize recognition in regions that align with the predicted future path.

### 3.3. Qualitative Analysis for Motion Focus

We conduct qualitative analysis on 30 video clips and select 3 representative scenes. Visual inspection reveals that the proposed motion focus mechanism operates robustly across diverse navigation scenarios, consistently highlighting motion-relevant regions.

As illustrated in Figure 5, the proposed motion focus consistently highlights motion-relevant regions across diverse egocentric scenarios. In Scene 1 (scooter), static but semantically salient objects such as parked vehicles are suppressed, while nearby obstacles along the walking path (e.g., poles, trees, and trash bins) are emphasized, demonstrating effective filtering of action-irrelevant visual clutter. In Scene 2 (walking), the predicted motion center adapts to vertical locomotion, shifting toward the ascending direction rather than remaining fixed at the image center. Furthermore, during Scene 3 (biking), when head orientation and body movement direction diverge, motion focus remains aligned with the torso-driven locomotion trend, prioritizing areas along the actual movement path.

## 4. Conclusion

This work shows that motion–driven analysis can serve as a lightweight and practical foundation for real-time egocentric perception, complementing existing action- and semantics-driven approaches in sports and fast-movement scenarios. More broadly, our findings suggest that grounding egocentric perception in physically significant motion is essential for understanding sports, robotics, and other dynamic embodied activities. By enabling lightweight, real-time ego-motion reasoning, this work takes a step toward more reliable and human-centered perception systems that

can support safety, performance analysis, and assistive feedback in challenging real-world environments.

## References

- [1] Masaki Fukuchi, Naotsugu Tsuchiya, and Christof Koch. The focus of expansion in optical flow fields acts as a strong cue for visual attention. *Journal of Vision*, 9(8):137–137, 2009. 3
- [2] Hassan A Karimi, Ming Jiang, and Rui Zhu. Pedestrian navigation services: challenges and current trends. *Geomatica*, 67(4):259–271, 2013. 1
- [3] Haotong Lin, Sili Chen, Junhao Liew, Donny Y Chen, Zhenyu Li, Guang Shi, Jiashi Feng, and Bingyi Kang. Depth anything 3: Recovering the visual space from any views. *arXiv preprint arXiv:2511.10647*, 2025. 1, 2, 3
- [4] Miao Liu, Siyu Tang, Yin Li, and James M Rehg. Forecasting human-object interaction: joint prediction of motor attention and actions in first person video. In *European conference on computer vision*, pages 704–721. Springer, 2020. 1
- [5] Minglang Qiao, Mai Xu, Shijie Wen, Lai Jiang, Shengxi Li, Tao Xu, Yunjin Chen, and Leonid Sigal. Saliency prediction of sports videos: A large-scale database and a self-adaptive approach. In *ICASSP 2024-2024 IEEE International Conference on Acoustics, Speech and Signal Processing (ICASSP)*, pages 6615–6619. IEEE, 2024. 1
- [6] Pei Sun, Henrik Kretzschmar, Xerxes Dotiwalla, Aurelien Chouard, Vijaysai Patnaik, Paul Tsui, James Guo, Yin Zhou, Yuning Chai, Benjamin Caine, et al. Scalability in perception for autonomous driving: Waymo open dataset. In *Proceedings of the IEEE/CVF conference on computer vision and pattern recognition*, pages 2446–2454, 2020. 1
- [7] Hao Wang, Jiayou Qin, Xiwen Chen, Ashish Bastola, John Suchanek, Zihao Gong, and Abolfazl Razi. Motor focus: Fast ego-motion prediction for assistive visual navigation. In *2024 IEEE 20th International Conference on Body Sensor Networks (BSN)*, pages 1–4. IEEE, 2024. 1, 3
- [8] Shuo Wang, Masaki Fukuchi, Christof Koch, and Naotsugu Tsuchiya. Spatial attention is attracted in a sustained fashion toward singular points in the optic flow. 2012. 3
- [9] Lingfeng Yang, Zhenyuan Chen, Xiang Li, Peiyang Jia, Liangqu Long, and Jian Yang. Agent-based video trimming. *arXiv preprint arXiv:2412.09513*, 2024. 1